Journal of Hazardous Materials 170 (2009) 219–229

Contents lists available at ScienceDirect

Journal of Hazardous Materials

journal homepage: www.elsevier.com/locate/jhazmat

Validation of two models for discharge rate

John L. Woodward *

Baker Engineering and Risk Consultants, Inc., 3330 Oakwell Ct., Ste. 100, San Antonio, TX 78118, United States

ARTICLE INFO

Article history:
Received 20 November 2008
Received in revised form 28 April 2009
Accepted 28 April 2009
Available online 5 May 2009

Keywords:
Discharge rate
Discharge models
Two-phase flow
Validation

ABSTRACT

A substantial body of discharge rate data has been developed over the past half century applicable for validation of single and two-phase discharge models. This paper applies a wide range of test cases and compares predictions with test data for two types of discharge model: (a) the energy balance model, and (b) the non-equilibrium model of Diener and Schmidt. The latter enhances the original homogeneous equilibrium model of Leung. This exercise reveals possible inconsistency between experimental datasets as much as it provides confirmation of the accuracy of the models, but both models are shown to provide adequate predictions within a factor of two and generally better.

1. Systems evaluated

The first step in process risk analysis is prediction of accidental discharge rates. The accuracy of this prediction is addressed here. The system evaluated is shown in Fig. 1. Discharges can be from a vapor line, a dip-leg (not shown), a liquid line, or a puncture on the vessel. In each case the source pressure P_0 is the stagnation pressure in the vessel, P_1 is the pressure at an intermediate point, P_C is the choke point, and P_2 is the ambient pressure or the back-pressure if the discharge is into another vessel. Reaction in the tank is not considered here.

2. Models evaluated

The SafeSite$_{3G}$® model of BakerRisk [1,2] has coded the energy balance (EB) model, and the non-equilibrium model (NEM) for calculating discharge rates, chosen as generally applicable for a wide range of pressure, temperature, and single- or multi-component mixtures. These models are evaluated here, comparing model predictions with experimental datasets. Discharge rates can be calculated for systems with a single phase (gas, vapor, or liquid), two-phases (flashing liquids or liquid with noncondensable gases) or three-phases (flashing liquids with solids). More accurate models may be available. The first step in improvements, though, is to establish how well predictions of given models compare with test data.

2.1. Energy balance model

Both the EB and the NEM use basically the same strategy for the more general case of pipe flow. That is, they both distribute the available pressure drop between the pipe pressure drop equation and the orifice discharge by varying an intermediate pressure P_1. The pressure drop across the pipe is P_0–P_1 with a mass flux through the pipe, G_P. The remaining pressure drop across the orifice is P_1–P_2 with a mass flux through the orifice of G_{ori}. At only one value of P_1 will G_P equal G_{ori}. That is, there is a root to the function:

$$f(P_1) = G_P - G_{ori} \tag{1}$$

This is readily established by the following reasoning. When P_1 is a minimum value equal to P_2, then G_{ori} is zero and G_P is at a maximum value, so $f(P_1 = P_2)$ is positive at a value of G_P. When P_1 is a maximum value equal to P_0 then G_P is zero so $f(P_1 = P_0)$ is a negative value of $-G_{ori}$. At an intermediate value of P_1, the curve of G_{ori} vs P and the curve of G_P vs P must cross and $f(P_1)$ must be zero.

The root-finding strategy evaluates G_{ori} from the energy balance across the orifice or pipe outlet and G_P from the momentum balance across the pipe. The differential momentum balance equation has terms for pressure drop across the pipe, $v\mathrm{d}P$, acceleration, friction losses, and potential energy gain from elevation changes $\mathrm{d}z$, where the angle θ is between the pipe break and the pump or tank:

$$v\mathrm{d}P + G_P^2 v\mathrm{d}v + \left[4f_L\frac{\mathrm{d}z}{D} + K_e\right]\frac{1}{2}G_P^2 v_L^2 \phi_L^2 + g\ \sin\theta \mathrm{d}z = 0 \tag{2}$$

The Fanning friction factor, f_L, is taken as the liquid phase friction factor, and is corrected for two-phase flow by the term ϕ_L^2. Commonly used correlations are used to find the value of f_L as a function of Reynolds number for the liquid. Let N_f collect the friction

* Tel.: +1 210 825 5960; fax: +1 210 824 5964.
E-mail address: Jwoodward@BakerRisk.com.

0304-3894/$ – see front matter © 2009 Elsevier B.V. All rights reserved.
doi:10.1016/j.jhazmat.2009.04.126

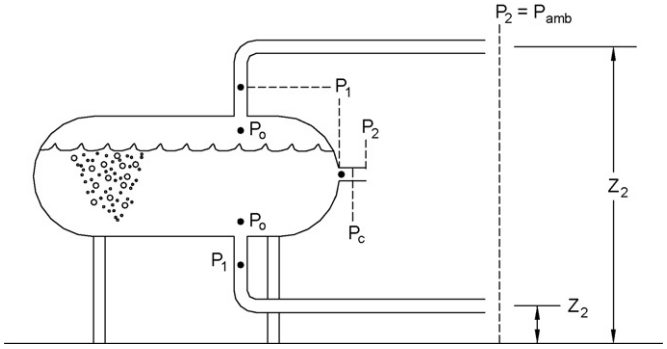

Fig. 1. Types of accidental discharge and pressure evaluation points.

loss terms in terms of the number of velocity heads, or:

$$N_f = 4f_L \frac{dz}{D} + K_e \tag{3}$$

where K_e is the number of equivalent head losses for pipe fittings, bends, valves, etc. The two-phase correction to friction factor is treated in texts [3].

The momentum balance is integrated numerically by assuming a value for G_P and stepping in increments of distance along the pipe to limits of either the pipe length, L, or the available pressure drop, P_0–P_1. When the latter limit is reached first, the value of G_P must be decreased. A converged value of G_P is found when the available pressure drop is realized at the actual pipe length.

After solving the momentum balance for the pipe mass flux, the program uses the value of P_1 suggested by the root finder and solves for the orifice mass flux, G_{ori}, using the energy balance equation. A numerical search is made to maximize the mass flux at a choke pressure, P_C between P_1 and P_2 or if the flow is subsonic, to maximize the flow over the pressure drop P_1–P_2.

Across planes 1 and 2, the general steady-state energy balance accounts for enthalpy change, kinetic energy, potential energy, heat inputs, and work outputs. Here H is specific enthalpy, J/kg, u is velocity, m/s, g is the gravitational constant, m/s^2, Δz is the elevation change from inlet to outlet, Q is heat transferred to the stream, W_p is the work done by the flow, and η_p, is work efficiency:

$$\Delta H + \frac{1}{2}u^2 + g \ \sin\theta \Delta z = Q - \eta_P W_P \tag{4}$$

Across an orifice, there is negligible heat transfer, no work is extracted, and negligible elevation change occurs, so the velocity is found directly from the enthalpy change assuming homogeneous flow and thermodynamic equilibrium:

$$u = \sqrt{2(H_1 - H_2)} \tag{5}$$

The assumption that the heat energy in enthalpy converts perfectly to kinetic energy (velocity) is idealistic and results in slightly high values of velocity and hence mass flux. Eq. (5) also places a premium on having an acceptable degree of accuracy for enthalpy correlations. The specific enthalpy can be written most generally, for three phases in terms of the mass fractions of vapor, x, and solids, x_s, and the specific enthalpies of vapor, H_v, liquid, H_L, and solids, H_{sol}:

$$H = xH_G + (1 - x - x_s)H_L + x_s H_{sol} \tag{6}$$

The mass fraction of solids remains constant while the vapor fraction x varies with pressure and saturation temperature. The assumption is generally made for discharges that ΔH is found along an isentropic expansion path. That is, as the pressure decreases from P_1 to P_2, the evaluation procedure is to select intermediate values of pressure, P_n. At each P_n find the temperature that keeps specific entropy, S, constant, T_{Sn}. Solve for the vapor fraction, x, using the entropy balance between planes 1 and n using the temperatures T_1 and T_{Sn}:

$$S_1 = xS_{Gn} + (1 - x - x_s)S_{Ln} + x_s S_{sol} \tag{7}$$

Since the mass fraction of solids is constant, the equilibrium vapor flash fraction is:

$$x = \frac{S_1 - [(1 - x_s)S_{Ln} + x_s S_{sol}]}{(S_{Gn} - S_{Ln})} \tag{8}$$

Find the enthalpies, H_1 at T_{S1} and H_2 at T_{S2} from physical property correlations and Eq. (3). Velocity is found from Eq. (5). The two- or three-phase density, ρ, is calculated from an equation of state at intermediate points P_n, T_{Sn} between P_1 and P_2 using a mass fraction weighted average of the specific volumes v_G, v_L, v_s (or the reciprocal of the corresponding phase densities, ρ_G, ρ_L and ρ_S) as functions of P_n, T_{Sn}. For example at point n:

$$\frac{1}{\rho_n} = v_n = x_n v_{Gn} + (1 - x_n - x_{sn})v_L + x_{sn} v_{sn} \tag{9}$$

Calculate the mass flux through the orifice from:

$$G_{ori} = u\rho = \frac{u}{v} \tag{10}$$

Search with values of P_n until G_{ori} is maximized. The choke pressure, P_C, is the value of P_n that produces a maximum value of mass flux, G_{ori}. The discharge rate, w, is given from the mass flux, a discharge coefficient, C_D, and the orifice cross-sectional area, A, as:

$$w = C_D A G_{ori} \tag{11}$$

In reality, equilibrium is achieved after a delay to allow for initiation and growth of bubbles. Hence, a correction can be applied for non-equilibrium to reduce the flash fraction at the choke point.

2.2. Non-equilibrium model (NEM)

The NEM of Diener and Schmidt [4,5] provides an analytical solution for both orifice and pipe flow. This model adds a term, N to adjust ω in the basic omega method or homogeneous equilibrium model (HEM) of Leung [6,7]. This term compensates for non-attainment of equilibrium conditions at the choke point.

Dimensionless values of pressure ratio, η, mass flux, G_*, and specific volume ratio, ε, are defined in terms of reference to the stagnation pressure, P_0. The dimensionless mass flux is defined in terms of the initial stagnation density, ρ_0, and P_0.

$$\begin{aligned} &\text{Pressure ratio}: \ \eta = \frac{P}{P_0} \\ &\text{Mass flux ratio}: \ G_* = \frac{G}{\sqrt{P_0 \rho_0}} \\ &\text{Specfic volume ratio}: \ \varepsilon = \frac{v}{v_0} \end{aligned} \tag{12}$$

In dimensionless variables, the momentum balance is:

$$\varepsilon d\eta + G_*^2 \varepsilon d\varepsilon + N_f \frac{1}{2} G_*^2 \varepsilon^2 \varphi_L^2 + \frac{g \ \sin\theta dz}{P_0 v_0} = 0 \tag{13}$$

The momentum balance equation can be analytically integrated after first relating the dimensionless specific volume, ε, to the dimensionless pressure ratio, η. A method to do this, designated the *omega method* was suggested by Leung [6] using:

$$\varepsilon = \begin{cases} \omega\left[\dfrac{\eta_s}{\eta} - 1\right] + 1 & \text{if } \dfrac{\eta_s}{\eta} > 1 \\ 1.0 & \text{if } \dfrac{\eta_s}{\eta} \le 1 \end{cases} \tag{14}$$

Eq. (14) represents a linear relationship between the two or three-phase specific volume and reciprocal pressure (v vs. P^{-1} or ε vs. η^{-1}) beginning at the bubble point or saturation pressure, P_S, where η is η_s. For single components, ω is found using the Clapeyron

equation to give a correlation in terms of the liquid heat capacity, C_{pL}, heat of vaporization, ΔH_{GL}, temperature, T, and pressure, P, and homogeneous two-phase specific volume v_0 from Eq. (9), all evaluated at the initial point, 0, or more precisely at the saturation point (point of initial flashing), η_S. If the liquid is initially at its saturation point, $\eta_S = 1$, so this is often assumed to obtain simpler formulas. When the non-equilibrium factor N is unity the NEM reduces to the homogeneous equilibrium model both in terms of the heat capacity of liquid, C_{PL0}, the temperature, T_0, pressure, P_0, heat of vaporization, ΔH_{GL0}, and specific volumes of vapor, v_{G0}, and liquid, v_{L0}, and two-phase mixture, v_0, at the stagnation point:

$$\omega = \frac{x_0 v_{G0}}{v_0} + \frac{C_{pL0} T_0 P_0}{v_0} \left(\frac{v_{G0} - v_{L0}}{\Delta H_{GL0}} \right)^2 N \tag{15}$$

The HEM has been found to generally under predict discharge rates, so the NEM was developed with the correction term defined by:

$$N = \left[x_0 + C_{PL0} T_0 P_0 \left(\frac{v_{GL0}}{H^2_{GL0}} \right) \ln \left[\frac{1}{\eta_C} \right] \right]^a \tag{16}$$

with

a = 0.6 for orifices, control valves, short nozzles (used in SafeSite$_{3G}$® coding)
a = 0.4 for pressure relief valves, high-lift control valves
a ~ 0 for long nozzles, orifice with large area ratio

An empirical expression has been found for the choke point pressure ratio:

$$\begin{aligned} &\eta_C = 0.55 + 0.217 \ \ln \omega - 0.046(\ln \omega)^2 + 0.004(\ln \omega)^3 \quad \text{if } \omega \geq 2 \\ &0 = \eta_C + \left(\omega^2 - 2\omega\right)(1-\eta_C)^2 + 2\omega^2 \ln(\eta_C) + 2\omega^2 (1-\eta_C) \quad \text{if } \omega < 2 \end{aligned} \tag{17}$$

The selection of choked or nonchoked flow is made by the simple logic:

$$\begin{aligned} &\text{If } \eta_2 \leq \eta_C \ \text{ then flow is choked, } \quad \text{use } \eta = \eta_C \\ &\text{Else subcritical, nonchoked flow, } \quad \text{use } \eta = \eta_2 \end{aligned} \tag{18}$$

The dimensionless mass flux for simple orifice flow for a saturated liquid ($\eta_s = 1$) is:

$$G^*_{ori} = \frac{\left[\omega \ \ln(1/\eta) - (\omega - 1)(1-\eta)\right]^{1/2}}{\left[\omega(1/\eta - 1) + 1\right]} \tag{19}$$

For pipe flow further logic is needed to treat the complications that occur because the saturation pressure may occur at the orifice or farther inside the pipe. That is, the saturation pressure can be below the stagnation pressure (η_s <1) generating a sub-cooled region from η_0 to η_s. The NEM solutions are stated below with a short-hand that recognizes that the denominator term in Eq. (14) is simply ε in Eq. (14).

Case 1 flashing in orifice, two-phase flashing flow in pipe

$$G^2_{*ori} = \frac{2\left\{(1-\eta_s) + \left[\omega\eta_s \ln(\eta_s/\eta_C) - (\omega-1)(\eta_s - \eta_C)\right]\right\}}{\varepsilon^2_C} \tag{20}$$

$$G^2_{*p} = 2\left\{ \frac{(\eta_1 - \eta_2)/(1-\omega) + (\omega\eta_s)/(1-\omega)^2 \ln((\eta_2\varepsilon_2)/(\eta_1\varepsilon_1))}{N_f + 2\ln(\varepsilon_2/\varepsilon_1)} \right\} \tag{21}$$

Case 2 sub-cooled liquid in orifice, flashing in pipe

$$G^2_{*ori} = 2(\eta_0 - \eta_1) \tag{22}$$

$$G^2_{*p} = 2\left\{ \frac{(\eta_1 - \eta_s) + (\eta_s - \eta_2)/(1-\omega) + (\omega\eta_s)/(1-\omega)^2 \ln(\eta_2\varepsilon_2)/(\eta_s\varepsilon_s)}{N_f + 2\ln(\varepsilon_2/\varepsilon_S)} \right\} \tag{23}$$

where for pipe flow, N_f is defined by Eq. (3). A more complete discussion is provided in texts [8].

As with the energy balance equations, the pressure drop across the system is distributed between a pressure drop across the pipe (from $\eta_0 = 1$ to η_1) and the pressure drop across the orifice (from η_1 to η_2). A root-finding routine finds the intermediate pressure ratio η_1 that gives the root of the function $f(G)$ defined by:

$$f(G) = G_{ori} - G_P \tag{25}$$

For a single-phase liquid, Eq. (20) reverts to the familiar orifice equation with $\varepsilon = 1$ (constant density), $\omega = 0$, $\eta_s = \eta_C = \eta_1$ giving:

$$G^2_{*ori} = 2(1 - \eta_1) \tag{26}$$

which reduces in dimensional form to the familiar form:

$$G = [2\rho_0 (P_0 - P_1)]^{1/2} \tag{27}$$

3. Single-phase discharge validation, sub-cooled liquids

Of necessity, the following comparisons were made in all but one case by using a single value of the pipe roughness factor, ε, of 1.5×10^{-6} m. The pipe roughness and liquid head in the system are usually not stated.

Uchida and Narai [9] used a single 4 mm ID pipe and successively shortened it, so the roughness length and other parameters are consistent. Their data for sub-cooled nonflashing water at 293 °K are shown in Figs. 2 and 3 compared with predictions of the EB model and the NEM, respectively. The results are essentially an ideal match. Statistics for all model predictions (bias and standard deviation) as listed in Table 3 can be considered to be the minimum achievable for both bias and standard deviation. For both models, with sub-cooled liquids, the models reduce to the orifice equation (Eq. (26)), and the orifice equation has long been recognized as accurate for single-phase liquids.

Uchaida and Narai also provide data at 300, 500, and 700 kPa (not shown) and the predictions for these pressures similarly match observations very well as well.

4. Sub-cooled temperature with flashing liquids

Model predictions are compared with experimental data in 26 additional plots that follow. Trend lines or data smoothing lines are added to nearly all of the observed data to aid comparisons.

Celata et al. [10] evaluated flashing water over a range of sub cooling below the saturation temperature. They evaluated source

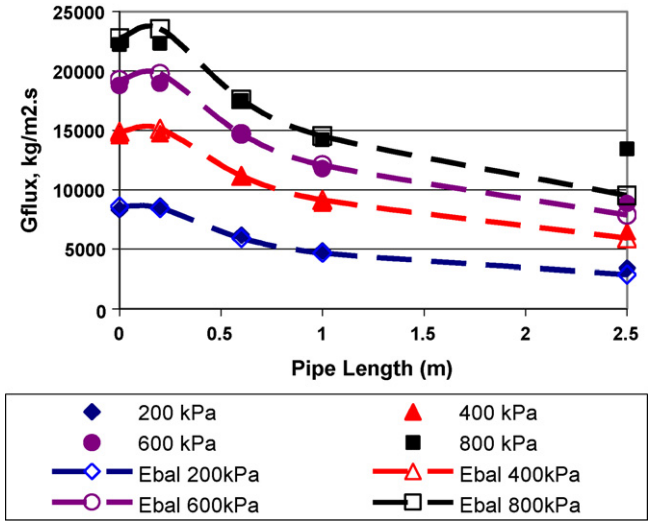

Fig. 2. Comparison of energy balance model with data of Uchaida and Narai for sub-cooled water.

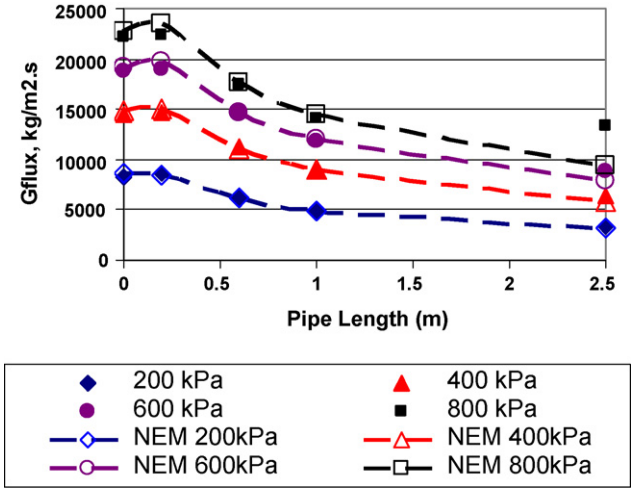

Fig. 3. Comparison of NEM with data of Uchaida and Narai for sub-cooled water.

pressures of 8, 15, and 23 barg with 4.6 mm diameter pipe at lengths of 46, 460, and 1380 mm. Discharge rate increases with increasing sub cooling both because the density increases and the flashing decreases. Fig. 4 plots data and predictions for the shortest pipe, and illustrates that the EB model over-predicts but has approximately the correct slope for mass flux vs degrees of sub cooling. The NEM under-predicts observations and has a lower sensitivity to sub cooling. Fig. 5, for the 460 mm pipe, and Figs. 6–8 for the 1380 mm pipe, show that the NEM predictions under-predict less as the pressure increases. Only in Fig. 6 is the NEM bias below a threshold of $-0.5\,\mathrm{kg/(m^2\,s)}$.

Sozzie and Sutherland [11] measured flashing water discharge rates for 12.7 mm ID pipe at temperatures around 540–550 K, just below saturation. The pressure was not held constant or varied monotonically. In Fig. 9, the EB model over predicts the data, but has the same sensitivity to pressure and pipe length as the data. The NEM under predicts and is less sensitive to pressure and pipe length than the data.

5. Saturated flashing liquids

Data of Uchaida and Narai [9] for saturated water are compared with predictions of the EB model and the NEM in Figs. 10 and 11. The limitation of assuming homogeneous equilibrium is apparent in Fig. 10, where for short pipes flashing has a large effect on discharge flux, so some sort of non-equilibrium correction is needed.

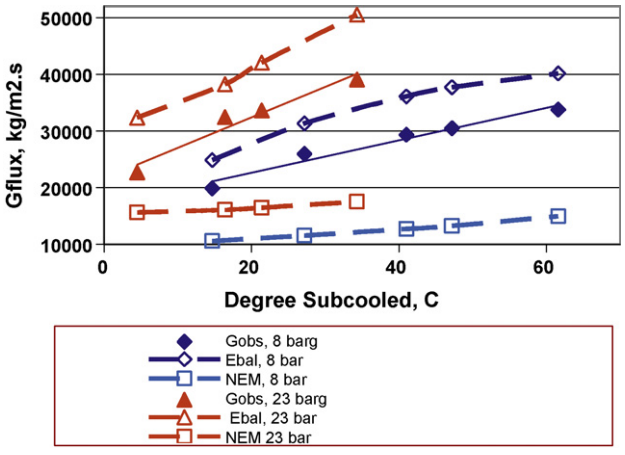

Fig. 4. Comparison of EB and NEM predictions with data of Celata et al. for 46 mm pipe length, varying pressure and sub-cooling.

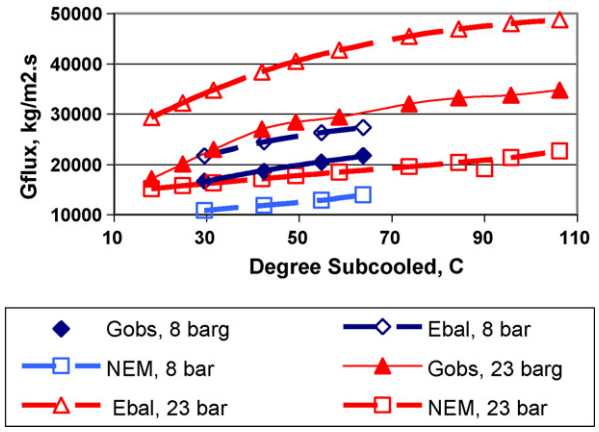

Fig. 5. Comparison of EB and NEM predictions with data of Celata et al. for 460 mm pipe length, varying pressure and sub-cooling.

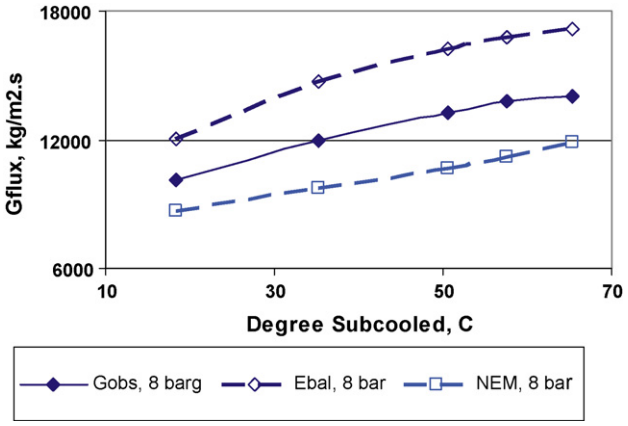

Fig. 6. Comparison of EB and NEM predictions with data of Celata et al. for 1380 mm pipe length, 8 barg.

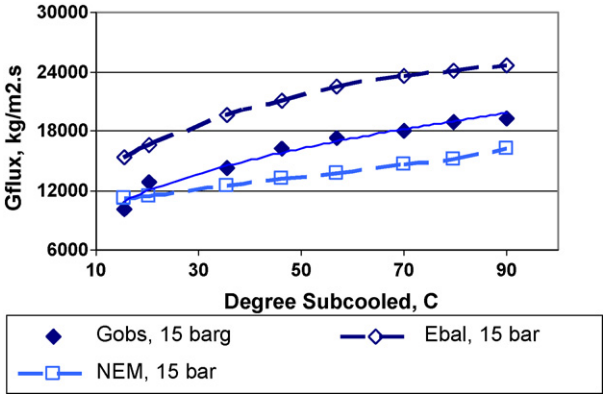

Fig. 7. Comparison of EB and NEM predictions with data of Celata et al. for 1380 mm pipe length, 15 barg.

The NEM model makes such a correction and has a better slope in the short pipe region in Fig. 11.

Van den Akker et al. [12] employed saturated refrigerant 12 (dichlorodifluoro-methane). The pipe lengths are quite short compared with those in Figs. 10 and 11, but are in the range where the mass flux drops rapidly with pipe length. As seen in Figs. 12 and 13, the slope of curves against pressure for both models agrees with observations. The spread between curves for the EB model is much less than that for the data. The NEM under predicts for short pipes (<30 mm) showing the non-equilibrium correction is not perfect,

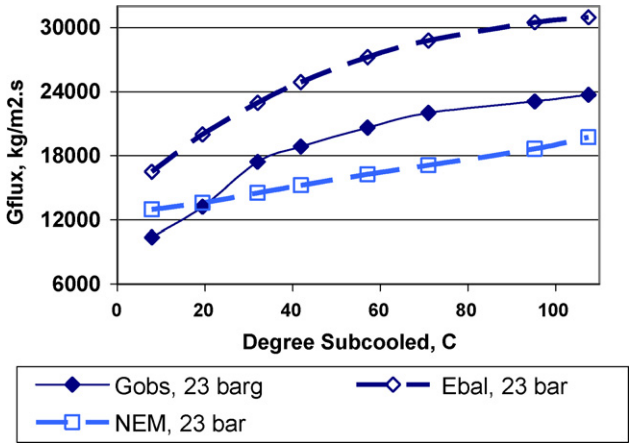

Fig. 8. Comparison of EB and NEM Predictions with Data of Celata, et al. for 1380 mm Pipe Length, 23 barg.

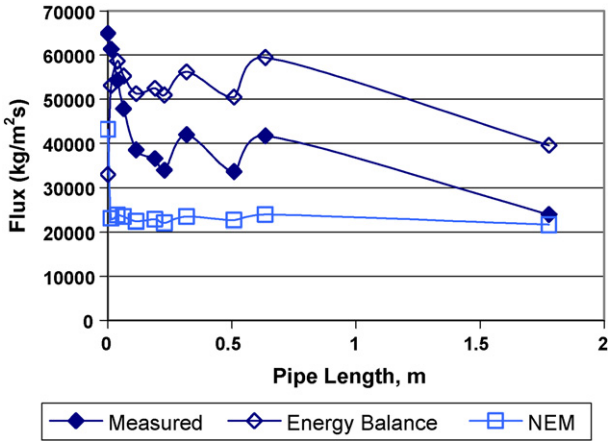

Fig. 9. Comparison of sub-cooled water data of Sozzie and Sutherland with predictions of two models (pressure varies).

but is acceptable for longer pipes where equilibrium in more nearly achieved.

Fig. 14 plots data by Burnell [13] with saturated water discharging into a vacuum. Both the EB and the NEM model under predict, but the EB statistics in Table 3 are slightly better than those of the NEM because of the under-prediction bias of the HEM, only partially corrected by the NEM.

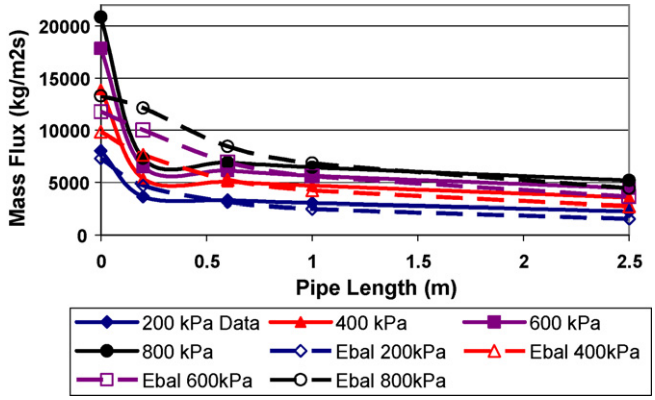

Fig. 10. Comparison of energy balance model predictions for saturated water with data of Uchaida and Narai.

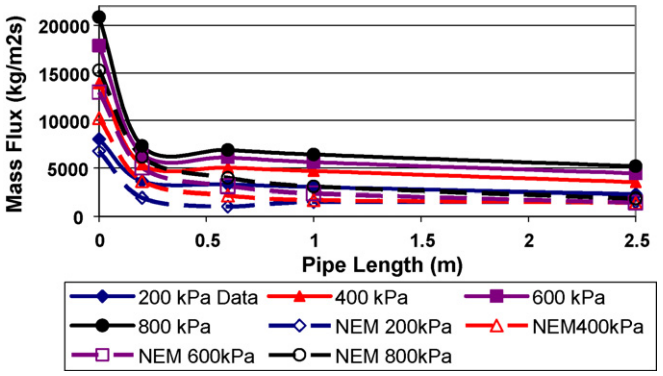

Fig. 11. Comparison of NEM predictions for saturated water with data of Uchaida and Narai.

Figs. 15–17 provide data by Fauske [14,15] for saturated water through short pipes against pressure. The EB model matches the 9 mm pipe length data very well while the NEM slightly under predicts. The NEM does very well with the 240 mm pipe length data while the EB model over predicts.

Fig. 18 treats saturated anhydrous ammonia data by Nyren and Winter [16] at pipe diameters of 32 and 40 mm, 1.96–4 m long. The pressures were 4.91 and 5.00 barg. Both models over predict, but the NEM predictions are considerably closer to the data.

In Fig. 19 the saturated water data of van den Akker and Bond [17] fall between the predictions of the EB model (slightly over predicting) and the NEM (slightly under predicting).

Fig. 20 shows data gathered by Schwellnus and Shoukri [18] including data from Al-Sahan [19] and Celata et al. [10] for saturated water at varying pipe length and diameter. Since several variables changed, the test conditions are listed in Table 1. The predictions of the EB model over predict. The NEM predictions range from very close to over-predicting.

Figs. 21 and 22 show data by Edwards [20] for saturated water over a wide range of pressure (200–2000 psia or 13.8–138 bar). The pipe diameter is 1/4 in. (6.35 mm). Pipe length is varied up to 0.9 ft (0.27 m). For the higher pressures, the observations in Fig. 22 generally fall between the model predictions. The EB over predicts and the NEM under predicts.

Figs. 23 and 24 have observations by Nielsen [21] for saturated water through three pipes of varying diameter and length as listed in Table 2. In this case, Nielsen provided two variables rarely reported, pipe roughness length and the height of liquid head. The lack of knowing these variables may be responsible for some of the variability between model predictions and experimental observations.

6. Superheated liquids

Figs. 25 and 26 show data by Fletcher [22] for a short pipe 2.86 mm long of 3.25 mm diameter with superheated flashing

Table 1
Test conditions by Schwellnus and Shoukri for saturated water.

Pipe diameter (mm)	Pipe length (m)	P_0 (bara)	T_0 (°K)	G_{obs} (kg/(m^2 s)
3.15	0.630	0.30	380.6	2443
3.15	0.630	4.79	430.8	3364
12.5	0.630	10.0	457.4	5157
12.5	3.60	34.9	517.3	10,090
3.15	0.270	66.3	556.3	33,930

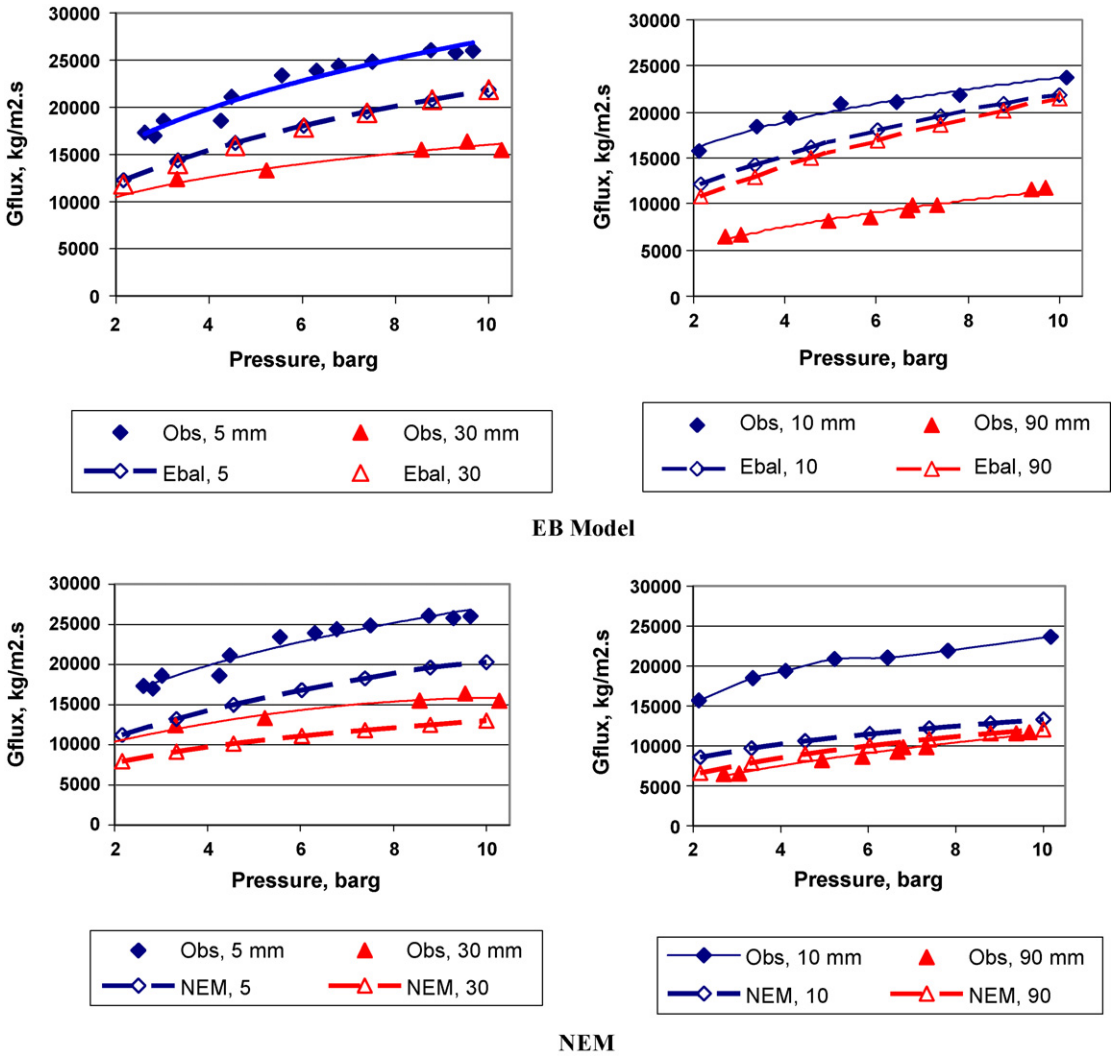

Fig. 12. Comparison of predictions with van den Akker data for saturated Freon 12, Part 1.

refrigerant 11 (CCl_3F). The predictions of both models compare reasonably well with the data.

In Figs. 27 and 28, additional data by Fletcher [22] for flashing refrigerant 11 are relatively insensitive to pressure. The EB model predicts higher discharge rates than the NEM and the NEM predictions fit the data better.

7. Bias and variance for datasets

The bias, $\bar{y}$, and standard deviation, σ, for each dataset and model are found by the standard formulas [23] for comparing predictions, $\hat{y}_i$, with observations, y_i, for n data points in a set:

$$\bar{y} = \frac{\sum_{i=1}^{n}(\hat{y}_i - y_i)}{n} \tag{28}$$

Table 2
Nielsen's test conditions.

Pipe no.	Pipe diameter (mm)	Pipe length (mm)	Pipe roughness (ε, mm)	ε/D
1	79.9	1840	0.024	0.0003
2	32.8	2000	0.013	0.000396
3	10.6	1840	0.013	0.001226

and

$$\sigma = \left[\frac{\sum_{i=1}^{n}(\hat{y}_i - y_i)^2}{n-1}\right]^{1/2} \tag{29}$$

Table 3 provides the bias and standard deviation, σ, for each set of predictions and data. The bias values for the NEM model are usually negative and below an absolute magnitude of 0.5 except for two points in Fig. 4 (flashing water).

The EB model bias is high, exceeding 0.5, for nine points (Figs. 12 and 13, flashing refrigerant 12; Fig. 17, flashing water; Fig. 18, flashing anhydrous ammonia, Fig. 20, saturated water; Fig. 23, saturated water; and Fig. 27, superheated refrigerant 11).

8. Summary and conclusions

Overall, this validation exercise confirms that the EB and NEM model are generally adequate. Usefully, these are particularly complimentary models since the EB model predictions are generally higher than those of the NEM, and together they provide a

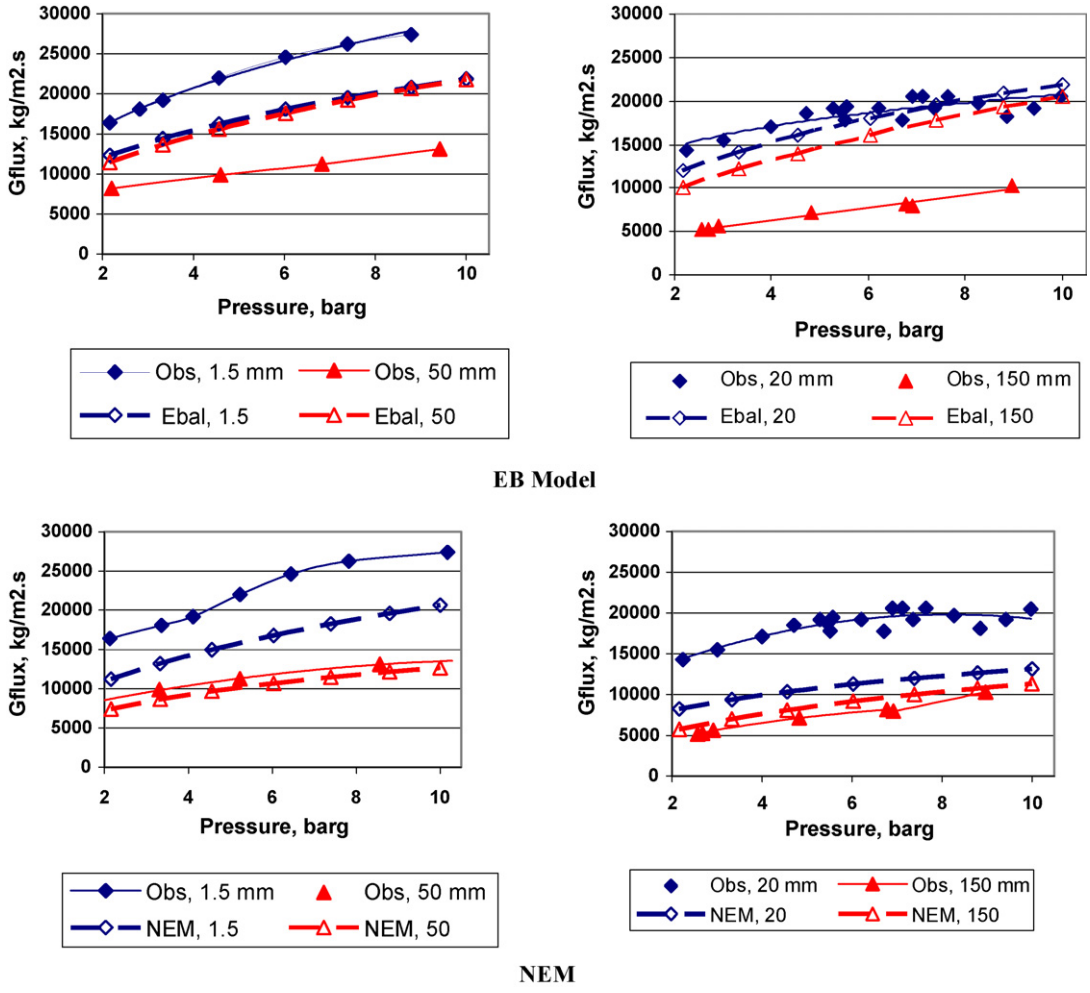

Fig. 13. Comparison of model predictions with data of van den Akker for saturated Freon 12, Part 2.

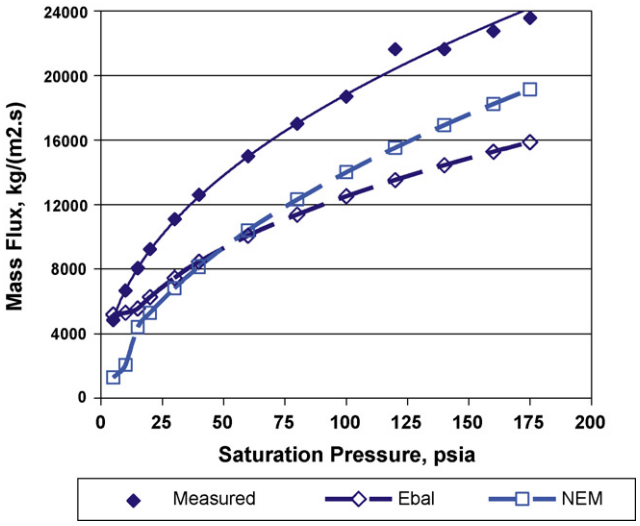

Fig. 14. Comparison of predictions with 0.213 in. orifice data of Burnell discharging saturated water into vacuum.

prediction range that indicates the uncertainty in model predictions.

There is enough variability in the experimental data that each model produces superior results for some datasets. As an evaluation aid, Table 4 combines the observations from the comparison plots provided above. The cases for which both model predictions match observations very well are:

- Figs. 2 and 3 (sub-cooled water)

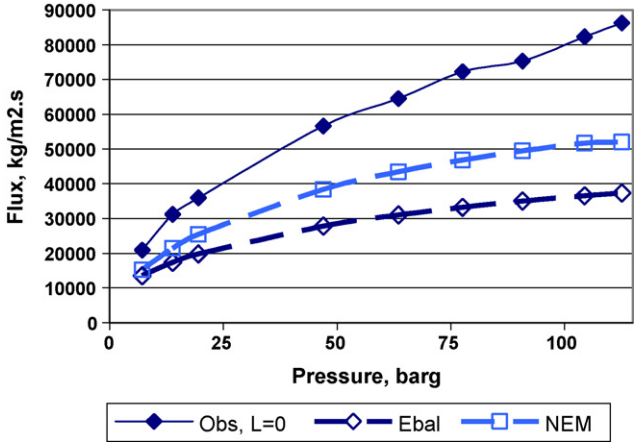

Fig. 15. Comparison of predictions with 6 mm orifice data of Fauske for saturated water.

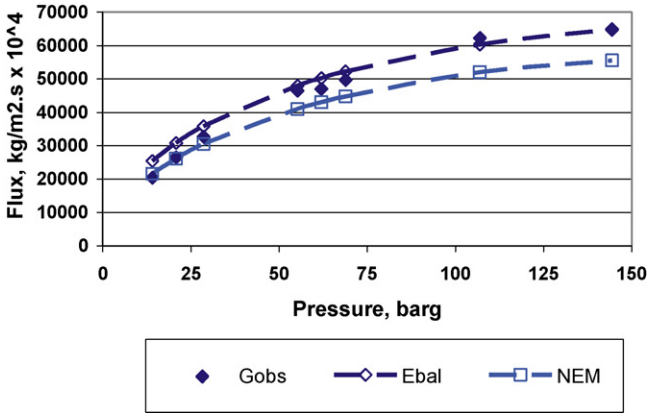

Fig. 16. Comparison of predictions with 6 mm diameter, 9 mm length data of Fauske for saturated water.

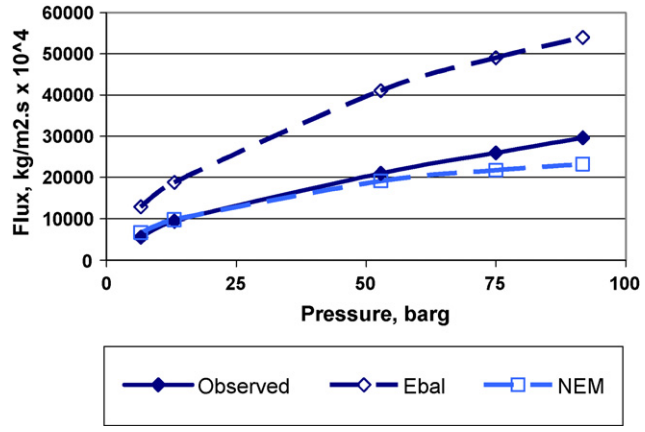

Fig. 17. Comparison of predictions with 6 mm diameter, 240 mm length data of Fauske for saturated water.

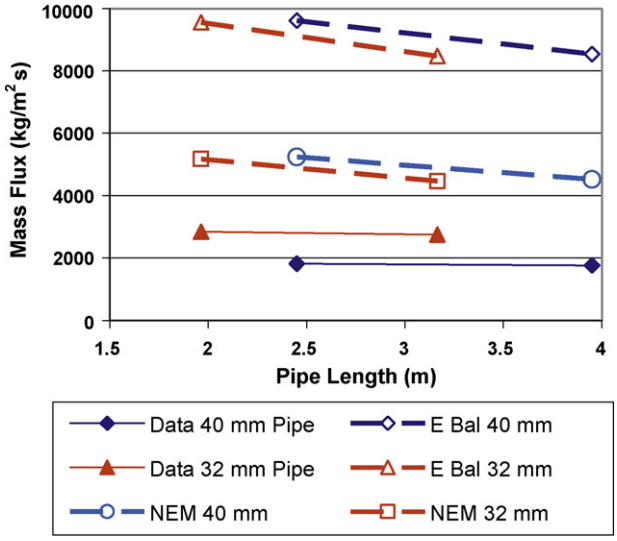

Fig. 18. Comparison of predictions with 32 and 40 mm diameter pipe with saturated anhydrous ammonia data of Nyren and Winter.

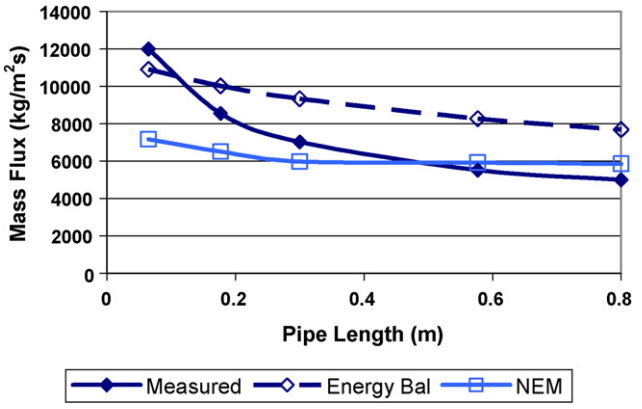

Fig. 19. Comparison of predictions with 49 mm diameter pipe with saturated water of van den Akker and Bond.

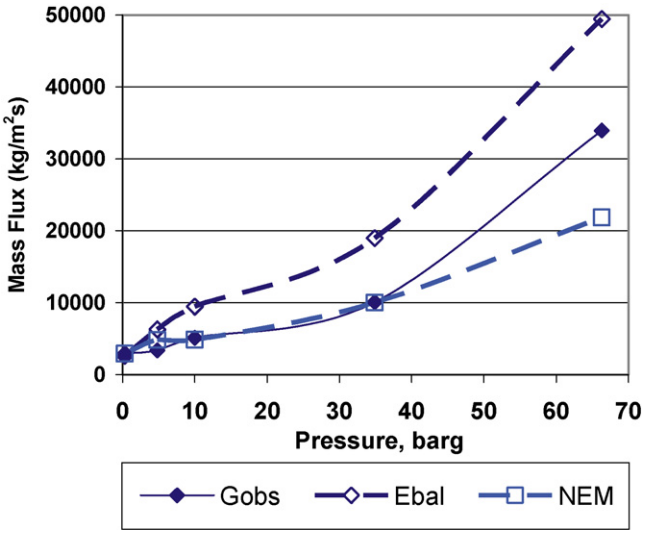

Fig. 20. Comparison of predictions for saturated water with data of Schwellnus and Shoukri for variable pipe diameter and length.

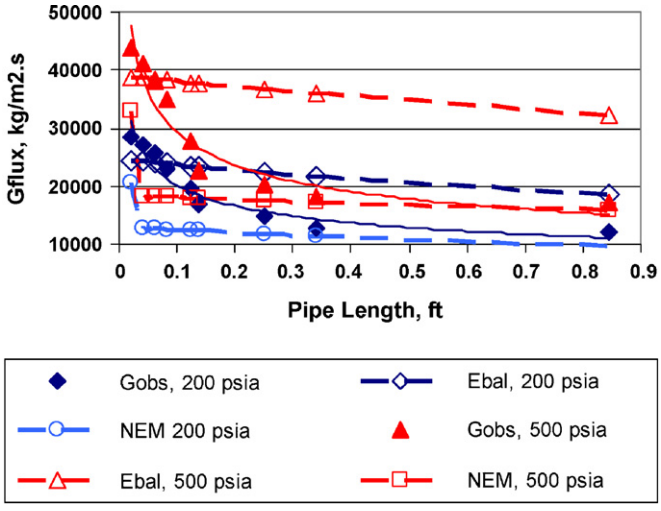

Fig. 21. Comparison of predictions for saturated water with data of Edwards varying pipe length and pressure 200–500 psia.

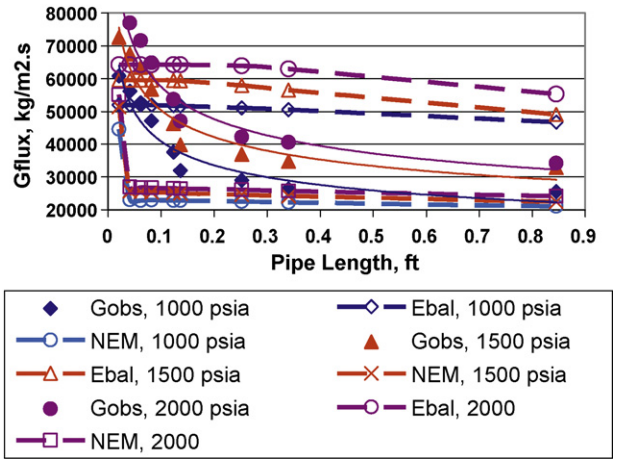

Fig. 22. Comparison of predictions for saturated water with data of Edwards varying pipe length and pressure 1000–2000 psia.

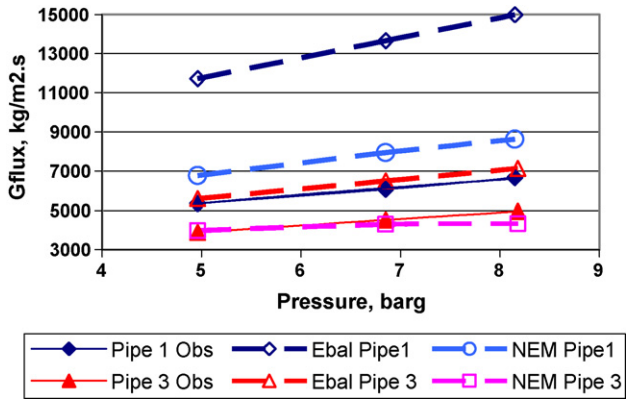

Fig. 23. Comparison of predictions for saturated water with data of Nielsen For varying pipe diameter, length, and pressure.

One model matches data very well for:

- Fig. 16 (EB model with saturated water)
- Fig. 17 (NEM for saturated water)
- Fig. 20 (NEM except at higher pressure)
- Fig. 23 (NEM model for Pipe 3)
- Fig. 24 (NEM for saturated water)
- Fig. 28 (NEM for flashing R11)

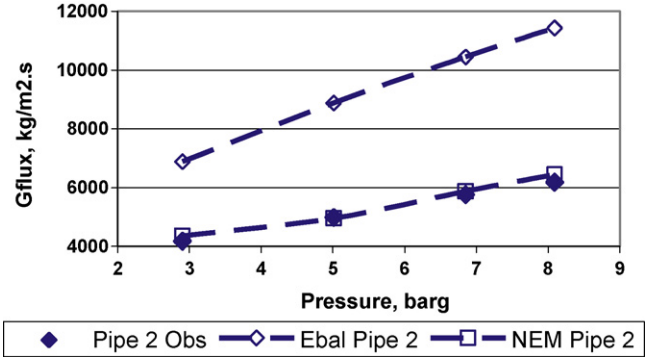

Fig. 24. Comparison of predictions for saturated water with data of Nielsen for varying pipe diameter, length, and pressure, Part 2.

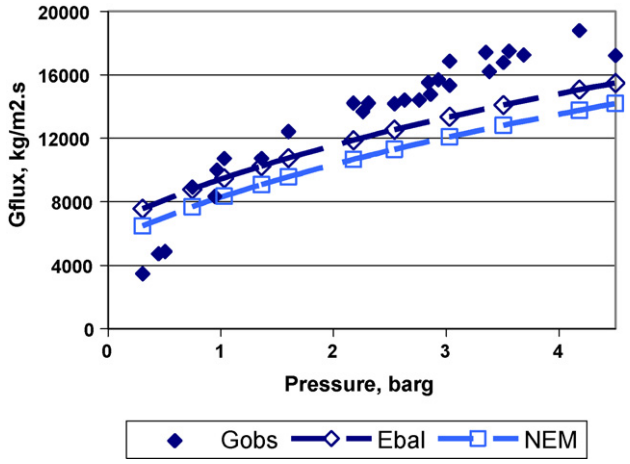

Fig. 25. Comparison with data of Fletcher for flashing refrigerant 11.

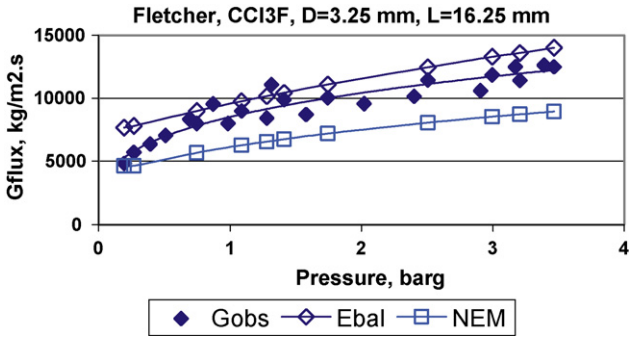

Fig. 26. Comparison with data of Fletcher for refrigerant 11 with 3.25 mm diameter, 16.25 mm length pipe.

Model predictions are good but not excellent for:

- Fig. 10 (EB with saturated water)
- Fig. 11 (NEM with saturated water)
- Figs. 12 and 13 (NEM with longer pipes for saturated Freon 12)
- Fig. 25 (EB and NEM for flashing R11)

The EB and NEM model predictions bracket the data for:

- Figs. 4–9

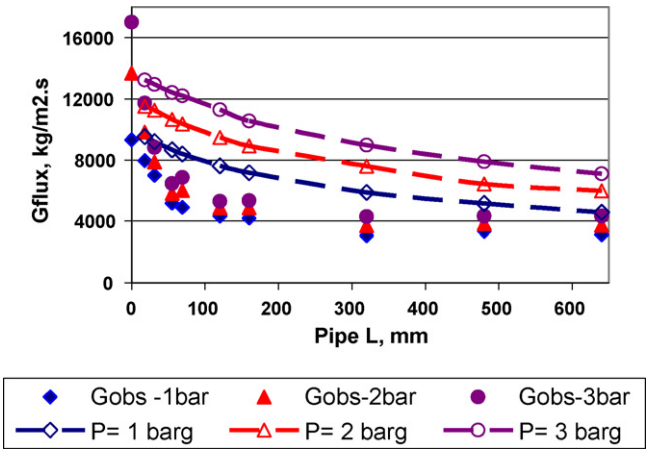

Fig. 27. Comparison of energy balance model with data of Fletcher for refrigerant 11.

Table 3
Summary comparison of bias and variance of model predictions.

Figure no.	Phase, fluid (authors)	Pressure (barg)	Pipe length (m)	Energy balance		NEM	
				Bias (kg/m^2 s)	SD	Bias (kg/m^2 s)	SD
2 and 3	Single-phase water (Uchaida and Narai)	2	0–2.5	−0.0421	0.0722	−0.0065	0.0357
		4	″	−0.0015	0.0437	−0.0049	0.0460
		6	″	−0.0034	0.0545	−0.0052	0.0555
		8	″	−0.0370	0.134	−0.0381	0.134
4 to 8	Flashing water vs sub-cooling (Celata et al)	8	0.046	0.222	0.250	−0.542	0.607
		15	″	0.290	0.318	−0.508	.0555
		23	″	0.287	0.347	−0.469	0.552
		8	0.460	0.281	0.335	−0.361	0.417
		15	″	0.475	0.552	−0.291	0.329
		23	″	0.478	0.515	−0.323	0.352
		8	1.380	0.217	0.243	−0.175	0.197
		15	″	0.327	0.358	−0.137	0.176
		23	″	0.374	0.415	−0.110	0.203
9	Flashing water (Sozzie and Sutherland)	63.8 to 64.8	0–1.78	0.255	0.427	−0.407	0.449
10 and 11	(Uchaida and Narai)	2	0–2.5	−0.0662	0.237	−0.435	0.524
		4	″	−0.0303	0.284	−0.478	0.561
		6	″	0.0293	0.338	−0.451	0.540
		8	″	0.0878	0.398	−0.402	0.490
12	Saturated refrig 12 (Van den Akker)	2 to 10	0.005	−0.228	0.251	−0.284	0.310
			0.030	0.231	0.271	−0.231	0.254
			0.010	−0.565	0.179	−0.444	0.481
			0.090	0.866	0.938	0.0994	0.123
13	″	2 to 10	0.0015	−0.251	0.277	−0.316	0.344
			0.050	0.576	0.628	−0.0394	0.0518
			0.020	−0.0330	0.116	−0.388	0.422
			0.150	0.989	1.07	0.131	0.159
14	Saturated water (Burnell)	−0.67 to 11.05	0	−0.290	0.323	−0.366	0.419
15	Saturated water (Fauske)	7.15 to 112.6	0	−0.496	0.531	−0.324	0.387
16	″	14.04 to 144.4	0.009	0.0776	0.121	−0.0793	0.111
17	″	6.6 to 91.7	0.240	0.991	1.123	−0.0477	0.174
18	Saturated NH_3 (Nyren and Winter)	4.91 to 5.00	1.96–3.95	3.15	3.80	1.23	1.54
19	Saturated water (van den Akker and Bond)	3.75	0.065–0.80	0.289	0.414	−0.110	0.263
20	Saturated water (Schwellnus and Shoukri)	0.30 to 66.3	0.27–3.6	0.587	0.782	0.0031	0.285
21 and 22	Saturated water (Edwards)	13.8	0.006–0.26	0.232	0.399	−0.326	0.376
		34.5		0.402	0.612	−0.293	0.366
		69		0.374	0.577	−0.353	0.410
		103		0.240	0.408	−0.427	0.472
		138		0.193	0.389	−0.466	0.511
23 and 24	Saturated water (Nielsen)	4.05 to 9.33	1.84–2.0	0.810	0.915	0.081	0.175
25	Superheated refrig 11 (Fletcher)	0.304 to 4.50	0.00286	−0.00046	0.394	−0.112	0.346
26	″	0.194 to 3.465	0.01625	0.215	0.265	−0.231	0.254
27 and 28	″	1	0.640	0.492	0.633	0.0680	0.275
	″	2	″	0.580	0.757	−0.0096	0.151
		3	″	0.643	0.846	−0.0177	0.161

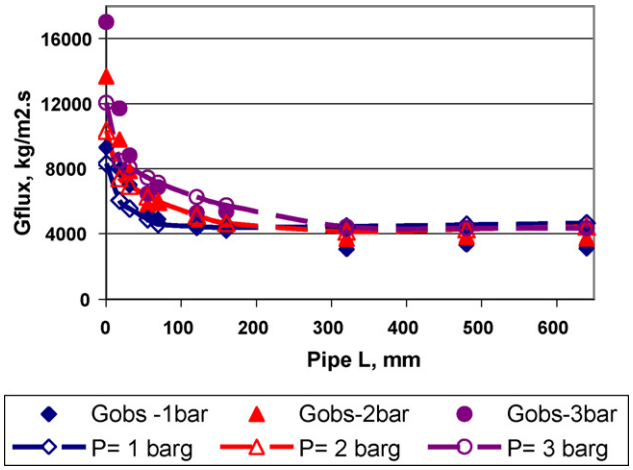

Fig. 28. Comparison of NEM with data of Fletcher for refrigerant 11.

- Fig. 19 (saturated water)
- Figs. 21 and 22 (saturated water)
- Fig. 26 (for flashing R11)

Both models under predict for:

- Fig. 14 (saturated water into vacuum)
- Fig. 15 (saturated water)

Both models over predict for:

- Fig. 18 (saturated anhydrous ammonia)
- Fig. 27 (EB for flashing R11)

Finally, experimenters are urged to provide the pipe roughness length and liquid head whenever possible.

Table 4
Summary comparison of model predictions with experimental data.

Figure no.	Phase, fluid (authors)	*G* Plotted against variable/parameter	Energy balance			NEM		
			Low	OK	High	Low	OK	High
2 and 3	Sub-cooled water (Uchaida and Narai)	*L*/*P*[a]		*X*			*X*	
4 to 8	Flashing water vs sub-cooling (Celata et al.)				*X*	*X*		
9	Flashing water (Sozzie and Sutherland)	*L*/*P*			*X*	*X*		
10 and 11	Saturated water (Uchaida and Narai)	*L*/*P*	sl *X*[b]	*X*		sl *X*	*X*	
12 and 13	Saturated refrig 12 (Van den Akker)	*P*/*L*	*X*	*X*	*X*	*X*	*X*	
14	Saturated water (Burnell)	*P*	*X*			*X* better		
15	Saturated water (Fauske)	*P*	*X*			*X* better		
16	″	*P*		*X*		sl *X*		
17	″	*P*			*X*		*X*	
18	Saturated NH_3 (Nyren and Winter)	*L*/*P*			*X*			*X* better
19	Saturated water (van den Akker and Bond)	*L*			*X*		*X*	
20	Saturated water (Schwellnus and Shoukri)	*P*/*L*,*D*			*X*		*X*	*X*
21 and 22	Saturated water (Edwards)	*L*/*P*			*X*	*X*		
23, 24	Saturated water (Nielsen)	*P*/*L*			*X*		*X*	
25	Superheated refrig 11 pipe (Fletcher)	*P*	sl *X* better			sl *X*		
26	″	*P*			*X*	*X*		
27 and 28					*X*		*X*	

[a] *D*: pipe diameter, *L*: pipe length, *P*: initial pressure.
[b] sl: slightly.

References

[1] Baker Eng. and Risk Consultants, Inc., SafeSite$_{3G}$™ Theory Manual, Version 1.04, April 28, 2005.
[2] Baker Engineering and Risk Consultants, Inc., SafeSite$_{3G}$™ Validation Manual, October, 2008.
[3] D. Chisholm, Two phase flow in pipelines and heat exchangers, G. Godwin, London in association with the Institute of Chemical Engineers, 1983.
[4] R. Diener, J. Schmidt, Sizing of throttling device for gas/liquid two-phase flow part 1: safety valves, Process Saf. Prog. 23 (December (4)) (2004) 335–344.
[5] R. Diener, J. Schmidt, Sizing of throttling device for gas/liquid two-phase flow part 2: control valves, orifices and nozzles, Process Saf. Prog. 24 (March (1)) (2004) 29–37.
[6] J.C. Leung, A generalized correlation for one-component homogeneous equilibrium flashing choked flow, AIChE J. 32 (1986) 1743–1746.
[7] J.C. Leung, Similarity between flashing and non-flashing two-phase flows, AIChE J. 36 (1990) 797–800.
[8] D.H. Green, R.H. Perry, Perry's Chemical Engineers' Handbook, 8th ed., McGraw Hill, NY, 2008, pp. 23–54 to 23–61.
[9] H. Uchida, H. Nariari, Discharge of saturated water through pipes and orifices, in: Proceedings of the 3rd International Heat Transfer Conference, vol. 5, Chicago, AssIChE, New York, NY, 1966, pp. 1–12.
[10] G.P. Celata, M. Cumo, G.E. Farello, Two-phase flow models in unbounded two-phase critical flows, Proceedings of the 3rd International Topical meeting on Reactor Thermal Hydraulics, Newport, RI, October, Am. Nuc. Soc. Paper 1F, 1985, pp. 1–6.
[11] G.L. Sozzi, W.A. Sutherland, Critical flow of saturated and subcooled water at high pressure, Nonequilibrium Two-Phase Flows, ASHE Winter Annual Meeting, Houston, TX, 1975 (More complete data in Report NEDO-13418, General Electric Co.).
[12] H.E.A. Van Den Akker, H. Snoey, H. Spoelstra, Discharges of pressurized liquefied gases through apertures and pipes, in: Proceedings of 4th International Symposium, September, Loss Prevention and Safety Promotion in the Process Industries, Harrogate, UK, 1983, pp. 12–16.
[13] J.G. Burnell, Flow of boiling water through nozzles, orifices, and pipes, Engineering (London) 164 (1947) 572.
[14] H.K. Fauske, Contribution to the theory of two-phase, one-component critical flow, Argonne Nat. Lab. Report ANL-6633, Oct, 1962.
[15] H.K. Fauske, The discharge of saturated water through tubes, Chem. Eng. Prog. Symp. Ser. 61 (1965) 210–216.
[16] K. Nyren, S. Winter, Two-phase discharge of liquefied gases through pipes, Field Experiments with Ammonia and Theoretical Model, National Defence Research Institute (Norway), Dept. 4, FOA Report B40139-31, January 1984.
[17] H.E.A. Van Den Akker, W.M. Bond, Discharge of saturated and superheated liquids from pressure vessels, Prediction of homogeneous choked two-phase flow through pipes, Symposium on the Protection of Exothermic Reactors and Presssurized Storage Vessels, Inst. of Chem. Eng. Symp. Ser., 85, 1984, pp. 91–108.
[18] C.F. Schwellnus, M. Shoukri, A two-fluid model for non-equilibrium two-phase critical discharge, Can. J. Chem. Eng. 69 (1991 Feb) 188–197.
[19] M.A. Al-Sahan, On the development of the flow regimes and the formation of a mechanistic non-equilibrium model for critical two-phase flow, Ph.D. Thesis, University of Toronto, 1988.
[20] A.R. Edwards, Conduction controlled flashing of a fluid and the prediction of critical flow rates in a one-dimensional system, Report AHSB(S) R147, UK Atomic Energy Authority, Health and Safety Branch, Risley, Warrington, Lancashire, UK, 1968.
[21] D.S. Nielsen, Validation of two-phase outflow model, J. Loss Prev. Process. Ind. 4 (July) (1991) 236–241.
[22] B. Fletcher, Flashing flow through orifices and pipes, in: AIChE 17th Loss Prevention Symposium, Denver, CO, August, 1983, pp. 28–31.
[23] G.E.P. Box, W.G. Hunter, J.S. Hunter, Statistics for Experimenters, John Wiley and Sons, NY, 1978, pp 40–41.